Active vibration control for thin curved structures using dielectric elastomer actuators

Toshiki Hiruta[1,*], Hiroki Ishihara[2], Naoki Hosoya[3], Shingo Maeda[4,5], Kentaro Takagi[1] Itsuro Kajiwara[6]

[1] Department of Mechanical Engineering, Toyohashi University of Technology

1-1 Hibarigaoka, Tempaku-cho, Toyohashi, Aichi, Japan

[2] Division of Human Mechanical Systems and Design, Hokkaido University

N13, W8, Kita-ku, Sapporo, Hokkaido, Japan

[3] Department of Engineering Science and Mechanics, Shibaura Institute of Technology

3-7-5 Toyosu, Koto-ku, Tokyo, Japan

[4] Department of Mechanical Engineering, Tokyo Institute of Technology

2-12-1, Ookayama, Meguro-ku, Tokyo, Japan

[5] Living Systems Materialogy (LiSM) Research Group, International Research Frontiers Initiative (IRFI), Tokyo Institute of Technology

2-12-1, Ookayama, Meguro-ku, Tokyo, Japan

[6] Division of Mechanical and Aerospace Engineering, Hokkaido University

N13, W8, Kita-ku, Sapporo, Hokkaido, Japan

[*] Corresponding Author

E-mail: hiruta.toshiki.kp@tut.jp

Abstract

This study proposes an active vibration control technique for pipe structures using dielectric elastomer actuators (DEAs). Vibrations in pipe structures must be eliminated to improve their mechanical reliability, and active vibration control techniques can be applied for effective vibration suppression. Soft actuators, which can completely fit pipe structures with complex-shaped surfaces, are required to transfer their vibration reduction forces to the target. DEA is suitable for this kind of target structure because DEA is characterized by high stretchability, flexibility, large deformation, and fast response. By applying the DEA, the effectiveness of vibration control for the pipe structure was experimentally demonstrated. A stacked DEA was fabricated and attached to the target structure. Its shape and placement were determined based on a modal analysis of the target structure. A control system, in which the controller for the active vibration control was designed based on H_∞ control theory, was composed. The vibration control experiment was conducted using the controller with a digital control system, and the vibration reduction effect was evaluated based on the frequency response of the target pipe structure.

Keywords: Dielectric elastomer actuator, Vibration experiment, Vibration control, Pipe structure, Modal analysis

1. Introduction

Structural failures of pipe structures are caused by vibrations owing to inner fluids or external disturbances. Lightweight pipe structures with thin walls are highly flexible. Their characteristic of low damping degrades their mechanical durability because the generated vibrations remain for a long duration. Pipe structures make significant contributions to ensuring the performance of vehicles and human safety. For example, pipe structures are installed in automobiles and trains to construct braking systems. In addition, exhaust gases are emitted from these structures. It is also through these structures that vessels are able to provide water to people. To improve their reliability, an active vibration control technique should be applied to pipe structures.

Lightweight and highly thin actuators are applied to the active vibration control of mechanical structures to ensure their performance. Conventionally, lead zirconate titanate (PZT) actuators[1–3] are used to reduce vibrations in mechanical structures[4]. Li et al. demonstrated a vibration control for the head stack of a hard disk drive using PZTs[5]. Shan et al. applied PZTs to reduce the vibrations of a flexible manipulator[6]. However, planner PZTs cannot be attached to structures with curved surfaces because of their high stiffness. Alternatively, polyvinylidene difluoride (PVDF) [7,8] and macrofiber composite (MFC) actuators[9,10] can be used owing to their mechanical flexibility. PVDF and MFC actuators are effective for application in simple cylindrical shells[11–13]. Zhang et al. demonstrated an adaptive vibration control technique for a cylindrical shell using a laminated PVDF actuator[11]. Sohn et al. verified the effectiveness of vibration control using MFC actuators for a hull structure based on the linear-quadratic-Gaussian (LQG) control theory[12]. Kwak et al. applied an MFC actuator and sensor in a vibration control experiment for a cylindrical shell[13]. When target objects are curved pipe structures with complex-shaped surfaces, PVDF and MFC actuators cannot fit them completely, leading to a decline in the vibration control effect. Herein, dielectric elastomer actuators (DEAs) can be adopted to pipe structures with complex surfaces because they are highly stretchable. In this study, a vibration control technique for pipe structures using DEAs was proposed. The target pipe structure was a simple cylindrical shell, which was used to assess the effectiveness of the proposed method as a fundamental study.

DEAs, which are composed of soft rubber-like polymeric materials sandwiched between stretchable electrodes[14–17], are activated by a voltage input[18,19]. DEAs are characterized by high stretchability, flexibility, large deformation, and fast response[20,21]. Many types of devices with DEAs that take advantage of these features have been developed[22–30]. Shintake et al. developed soft grippers composed of DEAs that can gently grasp objects[22]. Anderson et al. applied DEAs for the fabrication of flexible rotary motors[26]. Chen et al. demonstrated a miniaturized aerial robot that flies with flapping wings driven by DEAs actuation[27]. Maffli et al. developed DEA-integrated soft lenses that can change their focal length[28]. DEAs can generate vibrations at high frequencies owing to their fast responses[31–35]. Hosoya et al. demonstrated a balloon DEA speaker that generates sound pressure of up to 16 kHz[31]. Hiruta et al. obtained pear fruits' frequency responses of up to 2.5 kHz from vibration experiments using a DEA excitation technique[34]. Moreover, DEAs are effective for vibration control techniques for mechanical structures[36–41]. Sarban et al. demonstrated a tubular DEA between a shaker and a weight that can suppress the vibration of the weight[36]. Karsten et al. fabricated a stacked DEA consisting of 70 DE layers to isolate vibrations in its thickness direction[37]. Kajiwara et al. experimentally validated the effectiveness of a vibration control technique using a planner DEA[38]. Liu et al. analytically and experimentally proved the multi-layer DEA can improve vibration control effect for a thin cantilever plate[39,40]. Hiruta et al. applied a DEA to suppress the vibration of a membrane structure[42–44] subjected to noncontact laser excitation as an external disturbance[41,45–47]. Given these studies, the active vibration control effect using DEAs for structures with curved surfaces should be evaluated to further investigate the applicability of DEAs.

In this study, an active vibration control technique for pipe structures using DEAs is proposed. First, the actuation mechanism of the DEAs is described. Second, the fabrication procedure for stacked DEAs is presented. The DEAs contained multiple layers[39,48] to obtain sufficient excitation force for the target pipe structure. Herein, the shape and placement of the DEAs on the target structure, which were determined based on modal analysis, are shown. The modal analysis was performed based on a vibration experiment and numerical simulation. Subsequently, we elaborate on the active vibration control method for the pipe structure with the DEAs. A controller was designed based on the H_∞ control method, and a vibration control simulation was conducted for a modeled target pipe structure. Finally, a vibration control experiment using the controller and DEAs was conducted. The effectiveness of the proposed vibration control technique was evaluated experimentally.

2. DEA

2.1 Actuation mechanism

Figure 1 shows the actuation mechanism of the DEA. Stretchable electrodes are attached to both sides of the elastomer (Figure 1 (a)). The voltages applied to the electrodes on both surfaces of the elastomer generate the Maxwell stress, as expressed in Eq. (1).

$$P = \varepsilon_o \varepsilon_r \left(\frac{V}{d}\right)^2 \tag{1}$$

where ε_o and ε_r represent the vacuum and relative permittivities, respectively[20,49]. Meanwhile, V and d denote the applied voltage and the distance between the two electrodes, respectively. The strain in the thickness direction of the elastomer is expressed as

$$s_z = -\frac{1}{Y} \varepsilon_o \varepsilon_r \left(\frac{V}{d}\right)^2 \tag{2}$$

where Y is the elastic modulus and s_z is the thickness strain of the elastomer. Because an elastomer is considered as the incompressible approximatively in some application conditions, the mechanical constraint is written as

$$(1 + s_x)(1 + s_y)(1 + s_z) = 1 \tag{3}$$

where s_x and s_y denote the in-plane strains of the elastomer[50,51]. As shown in Figure 1(b), the Maxwell stress acting between the two electrodes compresses the elastomer in its thickness direction and expands it in the in-plane direction owing to the constraint expressed in Eq. (3). Therefore, the DEA can generate a stress in its in-plane direction. In this case, the elastomer is treated as an isotropic material. The DEA attached to the structure can apply bending stress on its surface and excite its vibration. To obtain sufficient excitation force, the DEA with multiple layers was applied to the vibration control experiment.

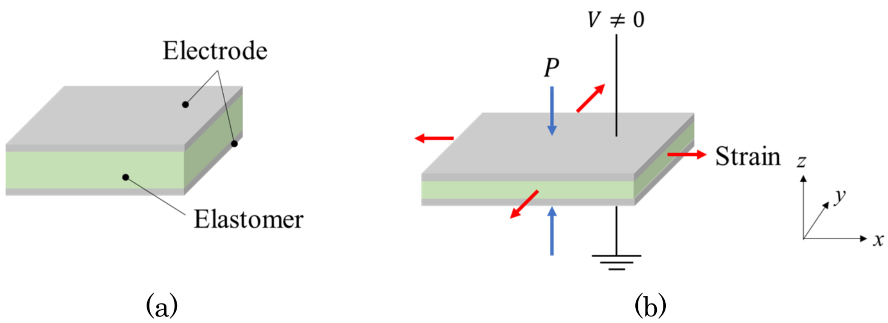

Figure 1 Actuation mechanism of the DEA. (a) The DEA is composed of an elastomer between stretchable electrodes. (b) A voltage activates the DEA. Maxwell stress P compresses the elastomer in its thickness direction and the elastomer expands in the in-plane direction owing to its incompressible characteristic.

2.2 Fabrication

Figure 2 shows the layers of the stacked DEA for the vibration experiment. The elastomers consisted of acrylic-based materials (VHB-4905J, 3M, 0.5-mm thick) and silicone-based materials (PDMS film 50-µm thick, Dow Toray, Japan, 0.05-mm thick). Carbon nanotubes (CNTs) were used as stretchable electrodes, whereas thin copper sheets were used as conducting wires. Each elastomer was stacked using a flexible adhesive (BBX, Cemedine)[35].

The fabrication procedure for the stacked DEA was conducted as follows. First, an acrylic elastomer, which has its own stickiness and can be attached directly to the target structure, was adopted as the base layer. Second, CNTs were coated onto the upper surface of the base layer. Third, a silicone elastomer was attached directly to the base layer using a flexible adhesive. The CNTs were then coated on the upper surface of the silicone elastomer. Herein, the silicone elastomer stacked on the base layer was sandwiched between two electrodes. Consequently, the voltage on each electrode activates the silicone elastomer, which is defined as the first active layer of the DEA. The second active layer was composed of another silicone elastomer sandwiched between two other electrodes and attached to the first active layer. Similarly, the third active layer was attached to the second active layer. Finally, the other silicone elastomer was attached to the top of the stacked active layers to preserve the stretchable electrodes. Copper sheets were attached to each stretchable electrode to obtain an input voltage. Figure 3 shows the dimensional geometry of the stacked DEA, with the shapes and dimensions determined based on the results of the modal analysis described in Section 3.3.

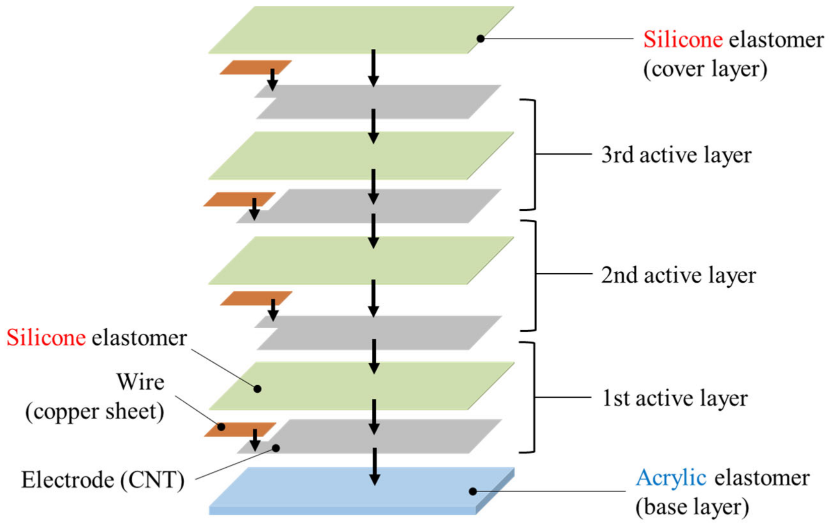

Figure 2 Layers of the stacked DEA for the vibration experiment. An acrylic elastomer, which has its own stickiness and can be attached directly to the target structure, was adopted as the base layer. Each active layer is composed of the silicone elastomer sandwiched between two electrodes. Active layers are actuated by applying voltages. A silicone elastomer is attached on top of the stacked active layers to conserve the stretchable electrode. Thin copper sheets were used as conducting wires.

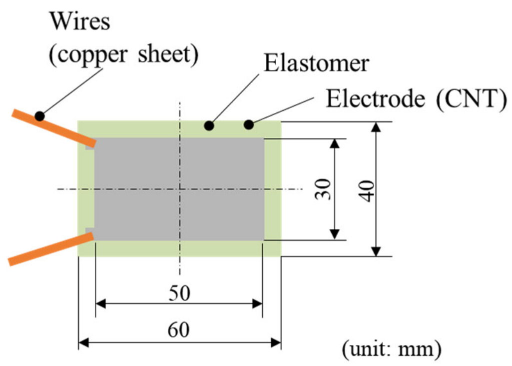

Figure 3 Dimensional geometry of the stacked DEA. The shapes and dimensions of the DEA is determined based on the result of the modal analysis.

3. Target structure

3.1 Pipe structure with DEAs

Figure 4 shows the dimensional geometry of the target structure for the vibration control experiment. The target was a pipe structure made of polyvinyl chloride (PVC) material. The length, outer diameter, and thickness of the pipe were 200 mm, 50 mm, and 1.0 mm respectively. Assuming a free-end bounding condition, both ends of the pipe structure were on the air cushions. Two fabricated DEAs, as shown in Section 2.2, were attached to the pipe structure directly and defined as DEA A and B. DEA A, which was attached to the outer surface of the target, was applied to conduct the vibration control. The placement of DEA A was determined based on the results of the modal analysis of the target structure, as described in the following section. The DEA B on the inner surface of the target was used for the disturbance input. A reflector was affixed to the measurement point on the outer surface of the pipe structure to measure the vibration responses in the direction normal to the target using a laser Doppler vibrometer (LDV; NLV-2500, Polytec). The sensitivity of the LDV was 5 mm/s/V.

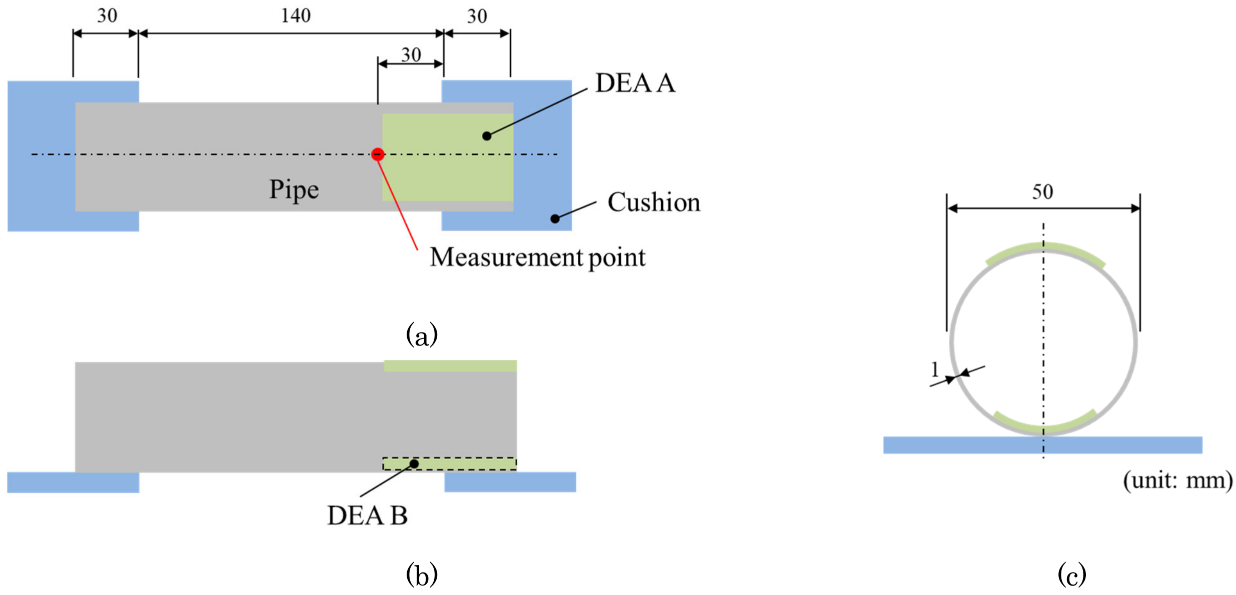

Figure 4 Dimensional geometry of the target pipe structure for the vibration control experiment. (a) Top view. (b) Front view. (b) Side view. Both ends of the pipe structure are on the air cushions, assuming a free-end bounding condition. Two DEAs are directly attached to the pipe structure and defined as DEA A and B. DEA A is applied to conduct the vibration control, whereas DEA B is used for the disturbance input. A reflector was affixed at the measurement point for vibration measurement using an LDV.

3.2 Mode shapes of the pipe structure

Modal analysis based on a finite element method (FEM) simulation and experimental modal analysis of the target pipe structure were conducted to determine the shape and placement of DEA A on the target.

The modal analysis based on the FEM simulation was performed using ANSYS. Table 1 lists the configuration of a finite element model of the pipe structure. The dimensional geometry of the model was similar to that in the experimental setup shown in Figure 4, including its thickness and the free-end bounding condition. The mode shapes and stress energy of the pipe structure were obtained from the simulation (Figure 5). The deformation and color contour of the finite element model correspond to the mode shape and modal strain energy distribution of the model, respectively. The blue and red colors in the model represent small and large strain energies, respectively. The shape and placement of the DEA A on the target were determined based on the distribution of the strain energy.

The experimental modal analysis was conducted to confirm mode shapes similar to those obtained numerically. Then, target vibration modes for the determination of the shape and placement of DEA A were selected. Figure 6 shows the vibration experiment system for the experimental modal analysis of the pipe structure. In this experiment, the DEAs were not attached to the pipe structure. An impulse hammer was applied to excite the vibration of the pipe structure, and the force signal from the impulse hammer was fed into the spectrum analyzer. The accelerometer was fixed to the outer surface of the pipe structure to measure the acceleration in the direction normal to its surface. The measured acceleration signal was input into the spectrum analyzer, and the frequency response between the force and acceleration signals was analyzed. Figure 7 shows the excitation points and the measurement point on the target structure. Excitation points were located on the surface of the pipe structure at 20-mm intervals in the longitudinal direction and 30° intervals in the circumferential direction. In this case, the impulse hammer cannot be applied to the bottom of the pipe structure on the air cushion. Therefore, the excitation points were located between 0° and 180° in the circumferential direction. Accordingly, the total number of excitation points on the pipe structure was 77, whereas the measurement point was fixed. The entire frequency responses obtained from the vibration experiment were curve-fitted, and the mode shapes of the pipe structure were extracted using ME'scope VES. Figure 8 shows the mode shapes of the pipe structure; the green and red colors in the model represent small and large deformations in the radial direction, respectively. The mode shapes obtained from the experimental modal analysis differ from the results of the FEM simulation shown in Figure 5 for each corresponding mode. The pipe structure used in the vibration experiment did not have an ideal cylindrical shape, and the air cushions and accelerometer affected the vibration characteristics. However, the mode shapes at the 1st and 3rd modes shown in Figure 8 are similar to the mode shapes at the 2nd and 5th modes in Figure 5.

The shape and position of the DEA A on the target arranged in this section provide a large difference in the strain energy between both ends of DEA A in the longitudinal direction of the pipe structure, particularly for the 2nd and 5th modes shown in Figure 5. DEA A can then obtain a large contribution from the control input to the target response during a vibration control experiment[38]. However, the difference in the strain energy between both ends of DEA A in the circumferential direction of the target was small because the position of DEA A was also determined to avoid target rolling.

Table 1. Configuration of the finite element model of the pipe.

Density	1300 kg/m^3
Young's modulus	0.3 GPa
Poisson's ratio	0.38
Nodal point	9568
Number of elements	1344

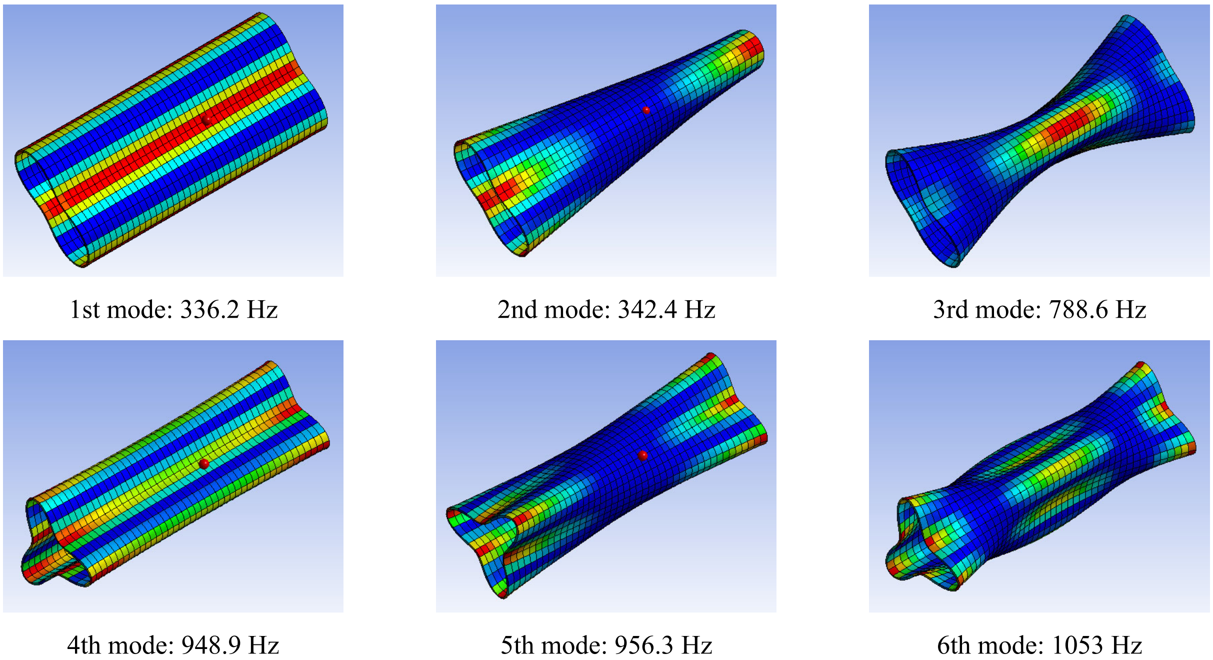

Figure 5 Mode shapes and stress energy of the pipe structure obtained from the numerical simulation in ANSYS. The deformation and color contour of the finite element model correspond to the mode shape and modal strain energy distribution of the model, respectively. The blue and red colors in the model represent small and large strain energies, respectively.

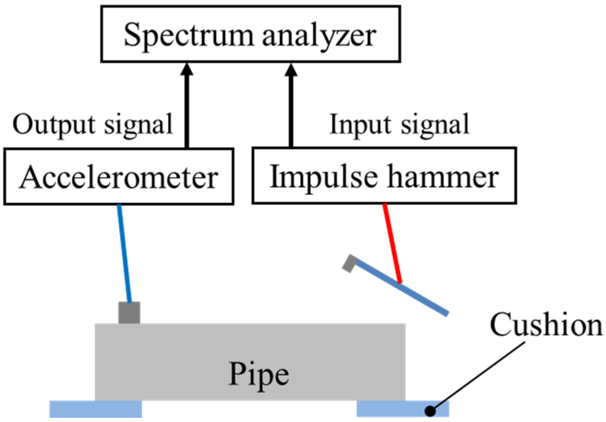

Figure 6 Vibration experiment system for the experimental modal analysis of the pipe structure. An impulse hammer is applied to excite a vibration of the pipe structure, and the force signal from the impulse hammer was fed into the spectrum analyzer.

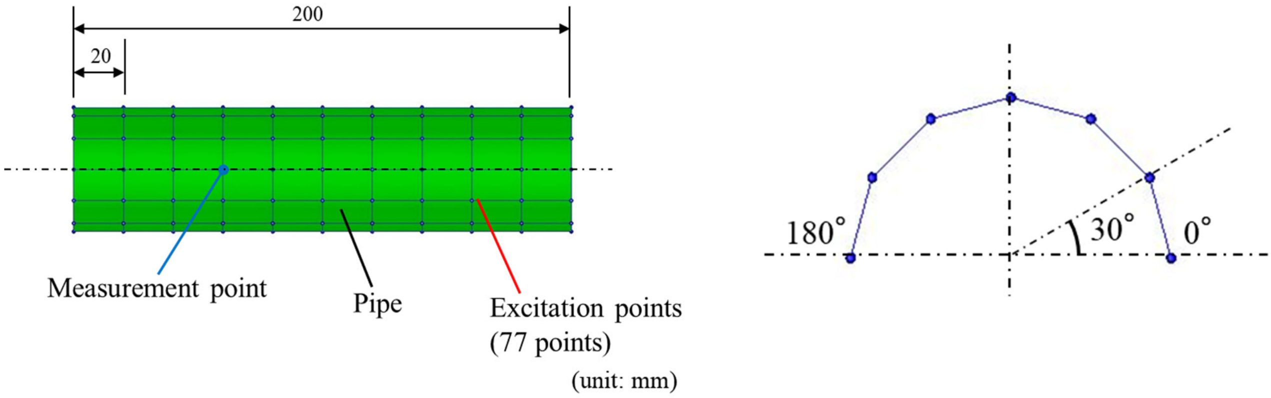

(a) (b)

Figure 7 Excitation points and measurement point on the target structure. Excitation points are located on the surface of the pipe structure in 20-mm intervals in the longitudinal direction and 30° intervals in the circumferential direction. (a) Top view. (b) Side view.

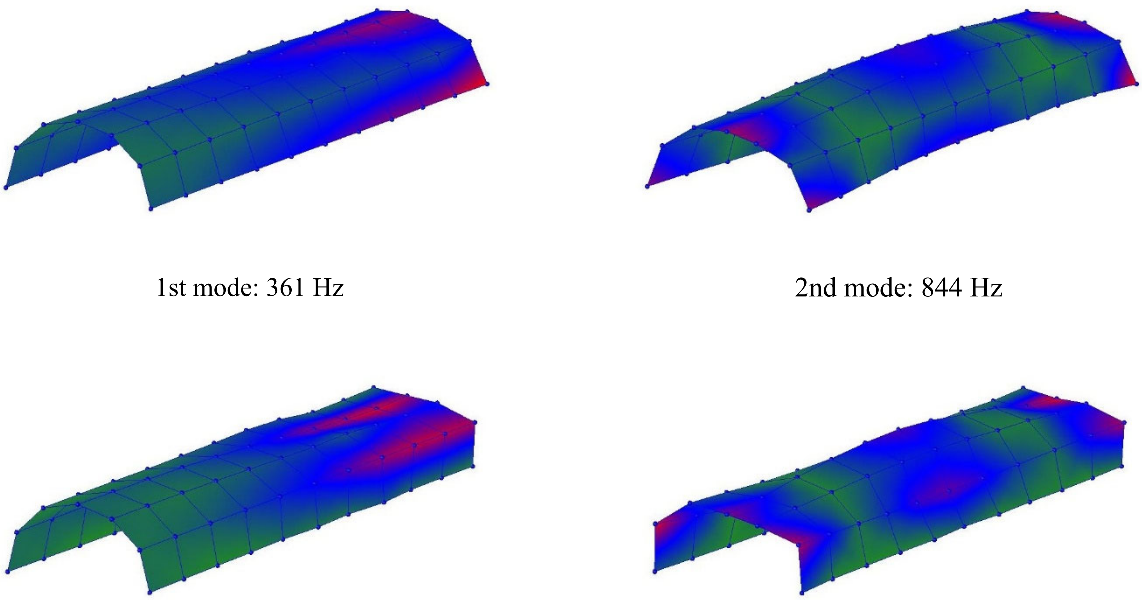

1st mode: 361 Hz

2nd mode: 844 Hz

3rd mode: 1010 Hz

4th mode: 1140 Hz

Figure 8 Mode shapes of the pipe structure obtained from the experimental modal analysis. The green and red colors in the model represent small and large deformations in the radial direction, respectively.

3.3 Measurement system for modeling

Figure 9 shows the vibration measurement system for creating a model of the target structure in the control system. A frequency response of the target structure was obtained from the vibration test, and the target was modeled based on the experimental modal analysis. The vibration measurement system was composed of the pipe structure with the DEAs, an LDV, a spectrum analyzer (A/D: NI PXI-4472B, National Instruments; Software: CAT-System, CATEC), signal generator

(33220A, Agilent Technologies), and high-output voltage amplifier (HVA-4321, NF, max voltage: ±10 kV). The details of the dimensional geometry of the target structure and the measurement point are shown in Figure 4.

The vibration test was conducted using DEA A to measure the frequency response of the target structure through vibration excitation. The signal generator produced a swept sine wave that was fed to DEA A via a high-output voltage amplifier. The amplitude, frequency range, and sweep time of the original swept sine wave were 0.5 V, 1–3000 Hz, and 2.56 s, respectively. The original swept sine wave was amplified 1000 times using the high-output voltage amplifier, resulting in an amplitude of 500 V. In addition, an offset voltage of 600 V was added to the amplified swept sine wave as the center voltage. The original swept sine wave (input signal) and the measured velocity signal from the LDV (output signal) were inputted into the spectrum analyzer. The analyzing frequency range and number of sampling points were 0–5000 Hz and 32768, respectively. Figure 10 shows the velocity output measured by the LDV.

Figure 11 shows the results of the vibration test. Distinct multiple resonance peaks are confirmed in the frequency range of 0–2000 Hz for the frequency response. The results indicate that the DEA can effectively transfer its excitation force to the target structure. The fast response of the DEA contributed to the vibration excitation for a wide frequency range. The resonance peak at 341 Hz corresponds to the 1st elastic mode of the pipe structure, considering the resonance frequency at the 1st mode shown in Figure 8. Similarly, other resonance peaks confirmed at frequencies greater than 500 Hz indicate the elastic modes of the pipe structure.

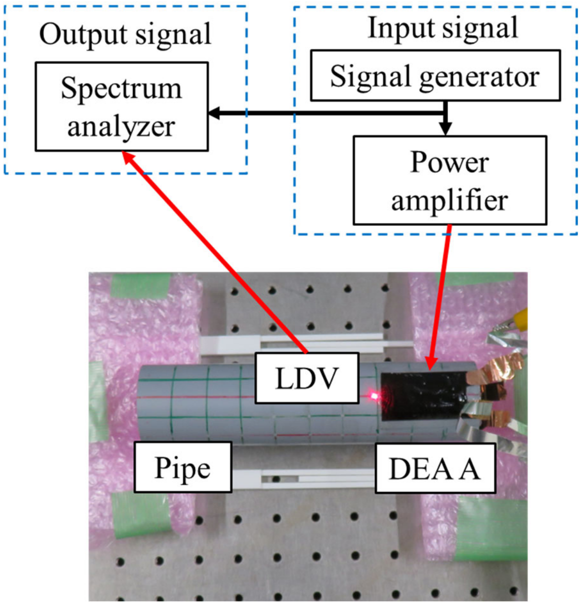

Figure 9 Vibration measurement system for creating a model of the target structure in the control system. The vibration measurement system is composed of the pipe structure with the DEAs, an LDV, a spectrum analyzer, signal generator, and high-output voltage amplifier.

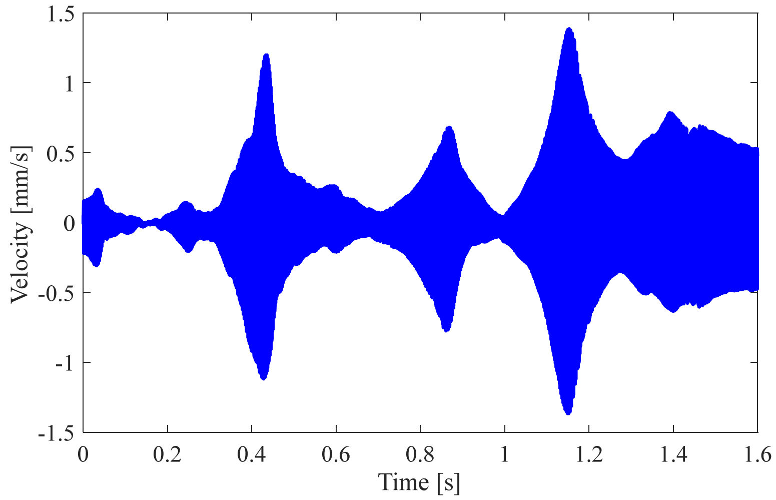

Figure 10 Time response of the velocity output. The velocity output is the target's vibration response measured using the LDV.

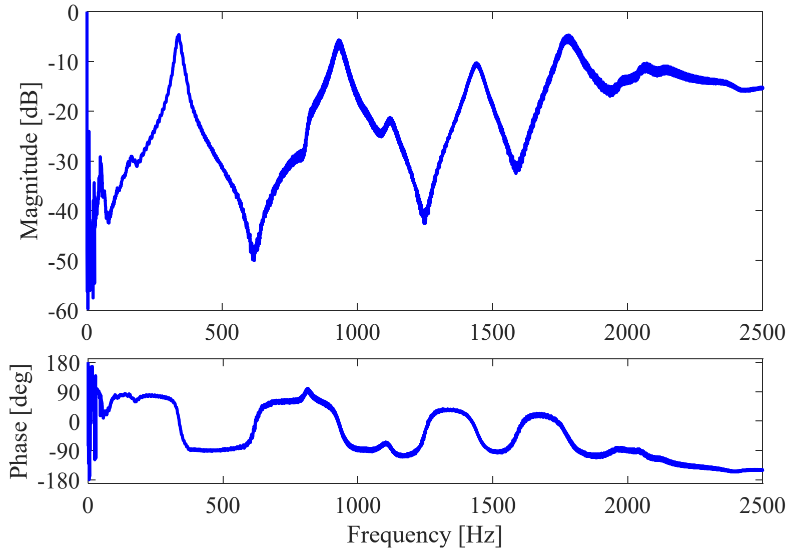

Figure 11 Frequency response of the pipe structure between the input signal and velocity output. The input signal is the original swept sine wave generated in the signal generator. The velocity output is the target's vibration response measured using the LDV. Distinct multiple resonance peaks are confirmed at the frequency range of 0–2000 Hz.

4. Controller design

4.1 Modeling of the pipe structure

System identification was applied to the frequency response shown in Figure 11 to create a model of the target. Here, it is assumed that nonlinear characteristics of the DEA due to their nonlinear elasticity can be ignored for the modeling process. Because the DEA's deformation in the vibration experiment was slight, a hysteresis of the DEA was assumed to be negligible.[52,53]. The frequency response function of the compliance is described as

$$G_{\mathrm{com}}(\omega)=\sum_{r=1}^{n}\left\{\frac{U_r+jV_r}{j(\omega-\omega_{\mathrm{dr}})+\sigma_r}+\frac{U_r-jV_r}{j(\omega+\omega_{\mathrm{dr}})+\sigma_r}\right\}+\frac{C}{\omega^2}+D \tag{4}$$

where ω is the angular velocity; r is the number of natural vibration modes; U_r, V_r, ω_{dr}, and σ_r, where $r=1,2,\cdots,n$, are the modal residues at the real part, modal residues at the imaginary part, damped natural angular frequency, and modal damping rate, respectively. C and D are the initial boundary and residual compliance, respectively, which compensate for the effects of the vibration modes omitted during system identification. Note that C and D are negligible because the effects of the omitted modes are assumed to be negligible in this study. These coefficients were identified through curve fitting based on the multipoint deviance iteration method applied to the frequency response shown in Figure 11. From Eq. (4), the transfer function $G_{\mathrm{com}}(s)$ is represented as a 2nd-order system of

$$G_{\mathrm{com}}(s)=\sum_{r=1}^{n}\frac{\eta_r s+\gamma_r}{s^2+\beta_r s+\alpha_r} \tag{5}$$

$$\begin{aligned}\alpha_r&=\sigma_r^2+\omega_{dr}^2,\beta_r=2\sigma_r\\ \gamma_r&=2(\sigma_r U_r-\omega_{\mathrm{dr}}V_r),\eta_r=2U_r\end{aligned} \tag{6}$$

where s denotes the Laplace operator. Subsequently, the transfer function in terms of rth-mode is transformed into the state-space equation in the observable canonical form, as described in the following expression:

$$\begin{aligned}\dot{\boldsymbol{q}}_{\mathrm{P},r}&=\boldsymbol{A}_{\mathrm{P},r}\boldsymbol{q}_{\mathrm{P},r}+\boldsymbol{B}_{1\mathrm{P},r}\boldsymbol{w}+\boldsymbol{B}_{2\mathrm{P},r}\boldsymbol{u}\\ &=\begin{bmatrix}0 & -\alpha_r\\ 1 & -\beta_r\end{bmatrix}\boldsymbol{q}_{\mathrm{eP},r}+\begin{bmatrix}\gamma_{1,r}\\ \eta_{1,r}\end{bmatrix}\boldsymbol{w}+\begin{bmatrix}\gamma_{2,r}\\ \eta_{2,r}\end{bmatrix}\boldsymbol{u}\\ \boldsymbol{y}_{\mathrm{P},r}&=\boldsymbol{C}_{\mathrm{P},r}\boldsymbol{q}_{\mathrm{P},r}\\ &=[0\quad 1]\boldsymbol{q}_{\mathrm{P},r}\end{aligned} \tag{7}$$

where $\boldsymbol{A}_{\mathrm{P},r}$, $\boldsymbol{B}_{1\mathrm{P},r}$, $\boldsymbol{B}_{2\mathrm{P},r}$, and $\boldsymbol{C}_{\mathrm{P},r}$ are coefficient matrices. $\boldsymbol{q}_{\mathrm{P},r}$, $\boldsymbol{w}$, and $\boldsymbol{u}$ denote the state, disturbance, and control input vectors, respectively. Because the disturbance input is assumed to be added to the control input in this study, the coefficient matrices $\boldsymbol{B}_{1\mathrm{P},r}$ and $\boldsymbol{B}_{2\mathrm{P},r}$ are rewritten as

$$\boldsymbol{B}_{1\mathrm{P},r}=\boldsymbol{B}_{2\mathrm{P},r}=\begin{bmatrix}\gamma_r\\ \eta_r\end{bmatrix} \tag{8}$$

The state-space equation including whole nth-degree of freedom system is expressed as

$$
\begin{aligned}
\dot{\boldsymbol{q}}_{\mathrm{P}} &= \boldsymbol{A}_{\mathrm{P}}\boldsymbol{q}_{\mathrm{P}} + \boldsymbol{B}_{1\mathrm{P}}\boldsymbol{w} + \boldsymbol{B}_{2\mathrm{P}}\boldsymbol{u} \\
&= \begin{bmatrix} \boldsymbol{A}_{\mathrm{P},1} & \cdots & \boldsymbol{0} \\ \vdots & \ddots & \vdots \\ \boldsymbol{0} & \cdots & \boldsymbol{A}_{\mathrm{P},n} \end{bmatrix} \begin{Bmatrix} \boldsymbol{q}_{\mathrm{P},1} \\ \vdots \\ \boldsymbol{q}_{\mathrm{P},n} \end{Bmatrix} + \begin{bmatrix} \boldsymbol{B}_{1\mathrm{P},1} \\ \vdots \\ \boldsymbol{B}_{1\mathrm{P},n} \end{bmatrix} \boldsymbol{w} + \begin{bmatrix} \boldsymbol{B}_{2P,1} \\ \vdots \\ \boldsymbol{B}_{2\mathrm{P},n} \end{bmatrix} \boldsymbol{u} \\
\boldsymbol{y}_{\mathrm{P}} &= \boldsymbol{C}_{\mathrm{P}}\boldsymbol{q}_{\mathrm{P}} \\
&= \begin{bmatrix} \boldsymbol{C}_{\mathrm{P},1} & \cdots & \boldsymbol{C}_{\mathrm{P},n} \end{bmatrix} \begin{Bmatrix} \boldsymbol{q}_{\mathrm{P},1} \\ \vdots \\ \boldsymbol{q}_{\mathrm{P},n} \end{Bmatrix}
\end{aligned} \tag{9}
$$

4.2 Control system design

Figure 12 shows a block diagram of the control system. $\boldsymbol{P}(s)$ is the transfer function converted from the state–space model described in Eq. (9). In the diagram, $\boldsymbol{y}_{\mathrm{P}}$ represents the output of the displacement, and the feedback signal in the vibration control experiment is the velocity signal outputted from the LDV. Therefore, an approximate differentiation filter is applied to convert the displacement into velocity and is expressed as follows:

$$
F_{\mathrm{vel}} = \frac{f_{\mathrm{v}} s}{s + f_{\mathrm{v}}} \tag{10}
$$

where f_{v} is a constant of the cutoff frequency, which is sufficiently higher than the control frequency range. In addition, the Padé approximations (Equation 11) was applied to compensate for the phase lag due to the discretization of the control system for the vibration control experiment.

$$
F_{\mathrm{pd}} = \frac{2 - Ls}{2 + Ls} \tag{11}
$$

L is a constant defined as

$$
L = \frac{f_{\mathrm{s}}}{2} \tag{12}
$$

where f_{s} is a sampling frequency of a discretized controller.

The state-space equation of the generalized controlled object $\boldsymbol{G}(s)$ in the control system (Figure 12) is expressed as

$$
\begin{aligned}
\dot{\boldsymbol{q}}_{\mathrm{G}} &= \begin{bmatrix} \boldsymbol{0} & \boldsymbol{0} \\ \boldsymbol{0} & \boldsymbol{A}_{\mathrm{G}} \end{bmatrix} \boldsymbol{q}_{\mathrm{G}} + \begin{bmatrix} \boldsymbol{0} \\ \boldsymbol{B}_{1\mathrm{G}} \end{bmatrix} \boldsymbol{w} + \begin{bmatrix} \boldsymbol{0} \\ \boldsymbol{B}_{2\mathrm{G}} \end{bmatrix} \boldsymbol{u} \\
\boldsymbol{y}_1 &= \begin{bmatrix} \boldsymbol{0} & \boldsymbol{0} \\ \boldsymbol{0} & \boldsymbol{Q}\boldsymbol{C}_{1\mathrm{G}} \end{bmatrix} \boldsymbol{q}_{\mathrm{G}} + \begin{bmatrix} \boldsymbol{R} \\ \boldsymbol{0} \end{bmatrix} \boldsymbol{u} \\
\boldsymbol{y}_2 &= \boldsymbol{C}_{2\mathrm{G}}\boldsymbol{q}_{\mathrm{G}}
\end{aligned} \tag{13}
$$

where

$$\boldsymbol{A}_{\mathrm{G}}=\begin{bmatrix}\boldsymbol{A}_{\mathrm{pd}} & \boldsymbol{B}_{\mathrm{pd}} & \mathbf{0} & \mathbf{0}\\ \mathbf{0} & \boldsymbol{A}_{\mathrm{vel}} & \mathbf{0} & \boldsymbol{B}_{\mathrm{vel}}\boldsymbol{C}_{\mathrm{P}}\\ \mathbf{0} & \mathbf{0} & \boldsymbol{A}_{\mathrm{vel}} & \boldsymbol{B}_{\mathrm{vel}}\boldsymbol{C}_{\mathrm{P}}\\ \mathbf{0} & \mathbf{0} & \mathbf{0} & \boldsymbol{A}_{\mathrm{P}}\end{bmatrix}, \boldsymbol{B}_{1\mathrm{G}}=\begin{bmatrix}\mathbf{0}\\ \mathbf{0}\\ \mathbf{0}\\ \boldsymbol{B}_{1\mathrm{P}}\end{bmatrix}, \boldsymbol{B}_{2\mathrm{G}}=\begin{bmatrix}\mathbf{0}\\ \mathbf{0}\\ \mathbf{0}\\ \boldsymbol{B}_{2\mathrm{P}}\end{bmatrix},$$
$$\boldsymbol{C}_{1\mathrm{G}}=[\mathbf{0} \quad \mathbf{0} \quad \boldsymbol{C}_{\mathrm{vel}} \quad \boldsymbol{D}_{\mathrm{vel}}\boldsymbol{C}_{\mathrm{P}}],$$
$$\boldsymbol{C}_{2\mathrm{G}}=[\boldsymbol{C}_{\mathrm{pd}} \quad \boldsymbol{D}_{\mathrm{pd}}\boldsymbol{C}_{\mathrm{vel}} \quad \mathbf{0} \quad \boldsymbol{D}_{\mathrm{pd}}\boldsymbol{D}_{\mathrm{vel}}\boldsymbol{C}_{\mathrm{P}}], \tag{14}$$

$\boldsymbol{A}_{\mathrm{vel}}$, $\boldsymbol{B}_{\mathrm{vel}}$, $\boldsymbol{C}_{\mathrm{vel}}$, $\boldsymbol{D}_{\mathrm{vel}}$ and $\boldsymbol{A}_{\mathrm{pd}}$, $\boldsymbol{B}_{\mathrm{pd}}$, $\boldsymbol{C}_{\mathrm{pd}}$, $\boldsymbol{D}_{\mathrm{pd}}$ are the coefficient matrices of the state-space equation of the approximate differentiation filter and the Pade approximation, respectively. $\boldsymbol{y}_1$ and $\boldsymbol{y}_2$ are the controlled value and observed output, respectively. $\boldsymbol{q}_{\mathrm{G}}$ represents the state vector of the generalized controlled object. $\boldsymbol{Q}$ and $\boldsymbol{R}$ are weighting matrices described as

$$\boldsymbol{Q}=\mathrm{diag}\left[w_z^{1/2} \quad \cdots \quad w_z^{1/2}\right]$$
$$\boldsymbol{R}=\mathrm{diag}\left[w_u^{1/2} \quad \cdots \quad w_u^{1/2}\right] \tag{15}$$

where w_z and w_u are the weighting coefficients.

The controller $\boldsymbol{K}(s)$ for suppressing the vibration of the target structure was designed based on the $\boldsymbol{H}_\infty$ control problem, which is described as

$$\min. \left\|\boldsymbol{T}_{y1w}\right\|_\infty \tag{16}$$

where $\boldsymbol{T}_{y1w}$ is the transfer function matrix between the disturbance input $\boldsymbol{w}$ and controlled value $\boldsymbol{y}_1$. The $\boldsymbol{H}_\infty$ norm of $\boldsymbol{T}_{y1w}$ is minimized by solving the H_∞ control problem using an approach based on the linear matrix inequality (LMI). The control system was designed using the Robust Control Toolbox in MATLAB.

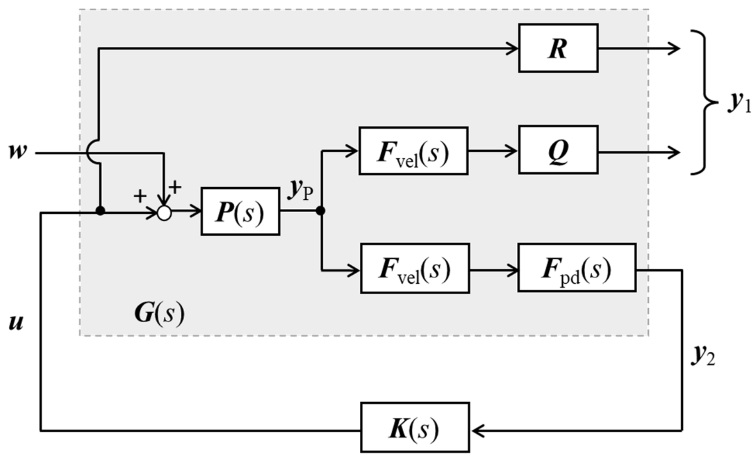

Figure 12 Block diagram of the control system. $\boldsymbol{w}$, $\boldsymbol{u}$, $\boldsymbol{y}_1$, and $\boldsymbol{y}_2$ are the disturbance vector, control input vector, controlled value, and observed output, respectively. $\boldsymbol{y}_{\mathrm{P}}$ represents the output of displacement. $\boldsymbol{P}(s)$, $\boldsymbol{K}(s)$, and $\boldsymbol{G}(s)$ are the state-space model, controller, and the generalized controlled object, respectively. $\boldsymbol{F}_{\mathrm{vel}}(s)$ and $\boldsymbol{F}_{\mathrm{pd}}(s)$ are the approximate differentiation filter and the Pade approximation, respectively. $\boldsymbol{Q}$ and $\boldsymbol{R}$ are the weighting matrices.

4.3 Vibration experiment system

Figure 13 shows the configuration of the vibration control system used in the experiment. The signal generator outputted a swept sine wave to activate DEA B via the high-voltage amplifier B. DEA B excited the vibration of the pipe structure, and the LDV measured the velocity in the radial direction at the measurement point of the target (Figure 4(a)). The velocity signal was fed to a digital signal processor (DSP) from the LDV. The disturbance input from the signal generator and the velocity signal from the LDV were also fed to the spectrum analyzer to obtain a frequency response. In the DSP, the analog velocity signal was converted into a digital signal and passed through a digital high-pass filter to remove the DC current component. Subsequently, a control signal was calculated in the discretized controller and converted into an analog signal. An offset voltage of 0.6 V was added to the control signal in the DSP. The control signal outputted from the DSP was then fed to DEA A via an analog low-pass filter and high-voltage amplifier A. The analog low-pass filter stabilized the control signal by reducing its gain over the control frequency range. Consequently, the amplified control signal activated DEA A to suppress the vibration of the target. Table 2 lists the specifications of the experimental system, which are sufficient for the vibration control and frequency response analysis in the target frequency range.

Table 2. Specifications of the experimental system.

Spectrum analyzer	Product	NI PXI-4472B, National Instruments
	Frequency range	0–5 kHz
	Sampling points	32768
	Overlap	15 samples
DSP	Product	WinCon 5.2, Quanser
	Sampling frequency	80 kHz
Analogue LPF	Product	3611, NF Corporation
	Cut-off frequency	4 kHz
Digital HPF	Order	1
	Cut-off frequency	25 Hz

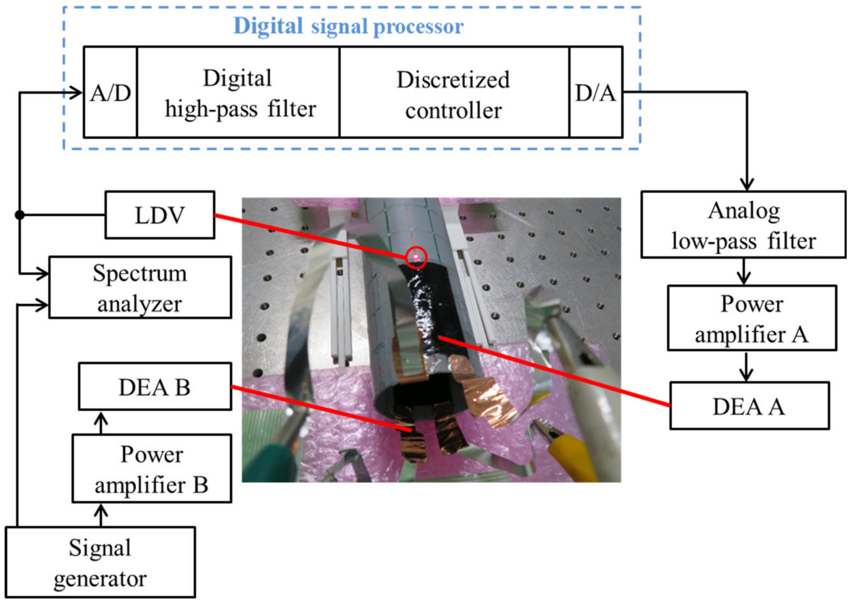

Figure 13 Control system diagram. The signal generator output a swept sine wave to activate the DEA B via the high-voltage amplifier B. The velocity signal is fed to the DSP from the LDV. A control signal is calculated in the discretized controller, and the control signal outputted from the DSP is fed to DEA A via an analog low-pass filter and high-voltage amplifier A. The amplified control signal activated the DEA A to suppress the vibration of the target.

5. Results and discussion

System identification was applied to the frequency response shown in Figure 11, and the natural frequencies f_r and modal damping ratios σ_r were identified, as listed in Table 3. In this study, the target vibration modes of the pipe structure are the 1st to 7th modes. The identified frequency response is presented in Figure 14. The model of the target structure was designed based on the system identification results and the procedure described in Section. 4.1. The control system was designed by selecting the constants described in Section. 4.2, as shown in Table 4. Subsequently, a vibration control simulation was performed in the control system using a designed controller with its frequency response shown in Figure 15. Figure 16 shows the vibration control simulation result, which is the calculated closed-loop frequency response of the observed output versus the control input disturbance. The vibration control effect is confirmed in the figure. In particular, the 1st, 3rd, and 6th vibration modes of the target structure showed reduced vibrations of 12 dB, 8 dB, and 11 dB, respectively.

A vibration control experiment was conducted using the system described in Section. 4.3. The controller in the vibration control simulation was discretized based on a first-order hold and applied to the DSP. Figure 17 shows the frequency responses between the disturbance input generated by the signal generator and the velocity signal. The 1st, 3rd, and 6th resonance peaks are reduced by 12 dB, 6 dB, and 5 dB, respectively. The resonance frequency in the 6th vibration mode varied during the vibration control, resulting in a decline in the vibration control effect. The remarkable vibration reduction effect on the 1st resonance peak was due to the appropriate placement and shape of DEA A, which was determined based on the distribution of the strain energy obtained from the modal analysis. Furthermore, the fast response of the DEA contributed to a reduction in the resonance peaks at frequencies greater than 1000 Hz. The DEA effectively transferred its control force to the target because it was completely attached to the curved surface owing to its high stretchability. The proposed vibration control technique using the DEA is effective for suppressing the vibrations of mechanical structures with curved surfaces.

Table 3. Identified modal parameters of the target structure.

Order	1st	2nd	3rd	4th	5th	6th	7th
f_r [Hz]	339.5	821.3	934.9	1127	1443	1774	2083
σ_r [$\times 10^{-3}$]	32.4	34.0	23.5	32.3	18.1	18.6	44.6

Table 4. Constants of the control system.

f_{v} [Hz]	5.0×10^5
f_{s} [Hz]	8.0×10^4
w_z	1.0×10^{13}
w_u	1.0×10^{12}

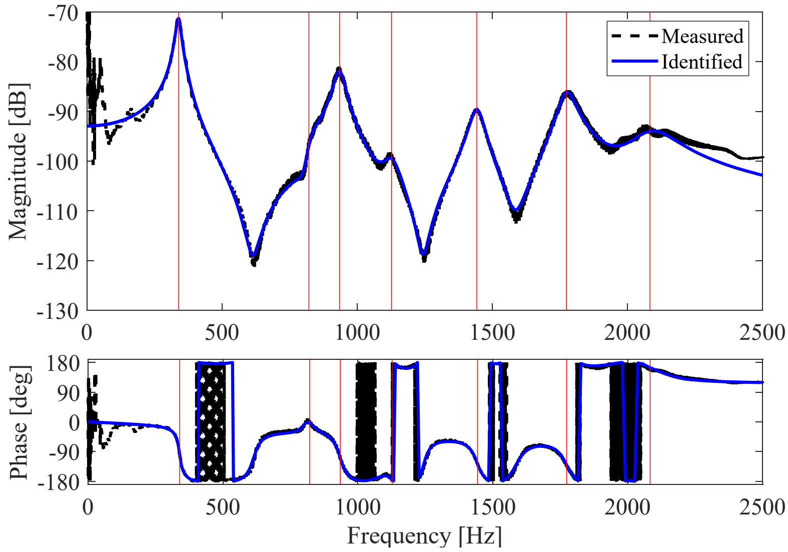

Figure 14 System identification results obtained by curve fitting using the multipoint deviance iteration method. Black dotted and blue solid lines indicate the measured and identified frequency responses, respectively.

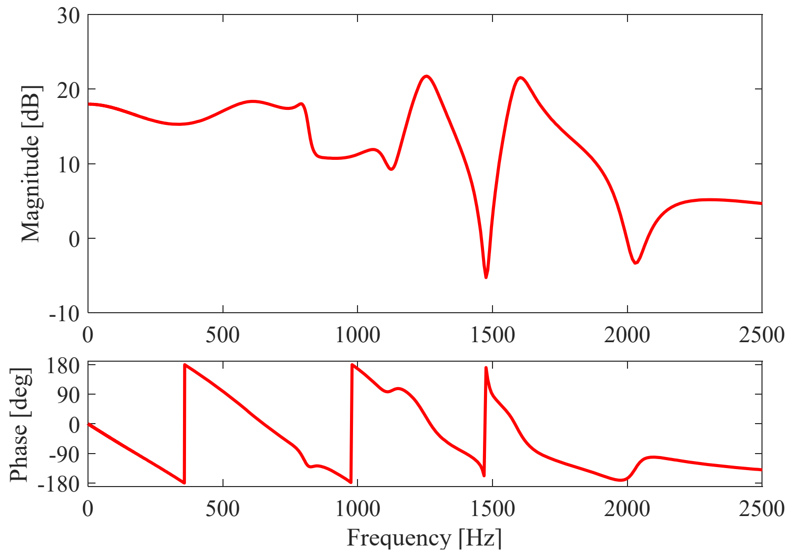

Figure 15 Frequency response of the controller based on the $\boldsymbol{H}_{\infty}$ control problem.

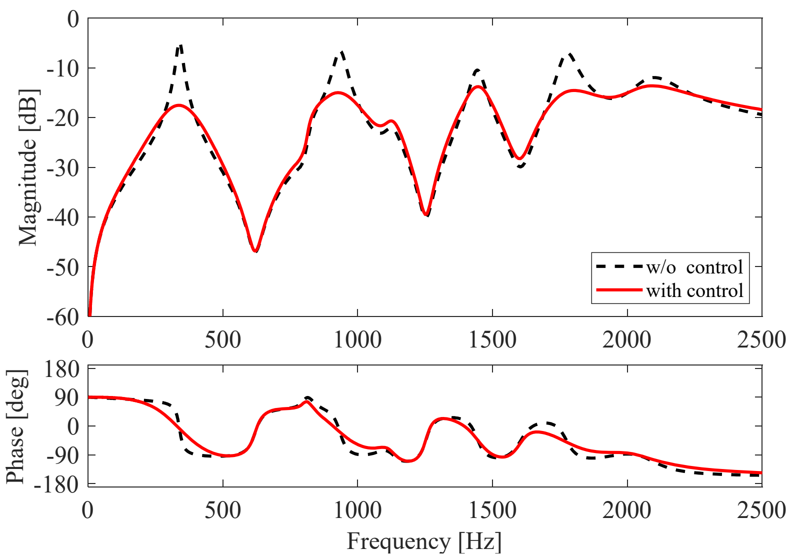

Figure 16 Calculated closed-loop frequency response of the observed output versus the control input disturbance. Black and red lines indicate the frequency responses with and without control, respectively.

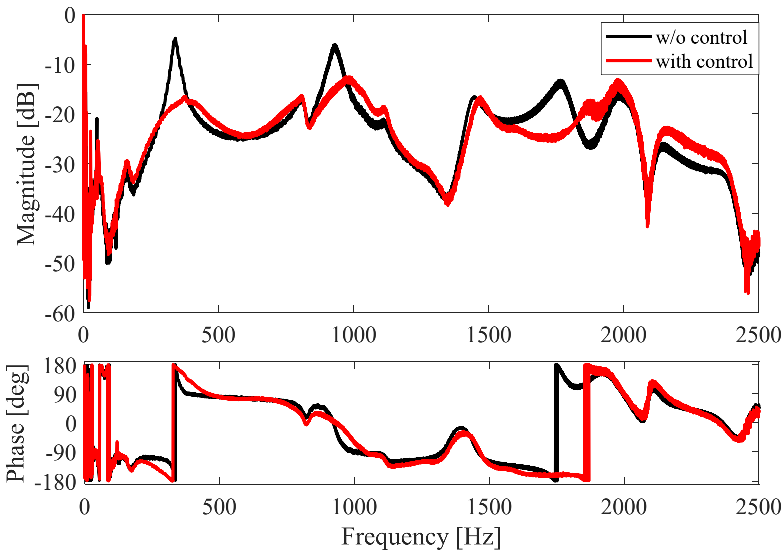

Figure 17 Measured frequency responses of the velocity output versus the disturbance input in the vibration control experiment for the target pipe structure. Black and red lines indicate the frequency responses with and without control, respectively.

6. Conclusions

In this study, a novel vibration control technique for pipe structures using DEAs was proposed. A DEA is a soft actuator composed of soft polymeric materials and flexible electrodes. Its high stretchability can be applied in vibration control techniques for mechanical structures. The stacked DEAs applied in the vibration control experiment in this study generated a sufficient excitation force based on Maxwell stress. A modal analysis was conducted for the target pipe structure to determine the shape and placement of the DEA on the target. The target structure was modeled through a vibration experiment, in which the DEA input was applied to design the control system. The controller was designed based on the H_∞ control problem, and the vibration control simulation was performed using the designed control system. Subsequently, the vibration control experiment was conducted, and the vibration reduction effect on the frequency response of the target was evaluated.

As a result of the vibration experiment, multiple resonance peaks of the target pipe structure were simultaneously reduced. The 1st, 3rd, and 6th resonance peaks are reduced by 12 dB, 6 dB, and 5 dB, respectively. The 1st resonance peak was significantly reduced owing to the appropriate placement and shape of the DEA, which generated a vibration control force on the target structure. The fast response of the DEA contributed to a reduction in the resonance peaks at frequencies above 1000 Hz. Owing to the high stretchability of the DEA, it completely attached to the target with the curved surface and effectively transferred its control force to the target. Thus, the effectiveness of the proposed vibration control technique using DEAs was experimentally validated. In the future, we plan to apply the proposed technique to structures with more complex curved surfaces. Moreover, LDV should be replaced with dielectric elastomer sensors (DESs) to create miniaturized vibration control systems.

Acknowledgments

This work was partially supported by the JSPS Kakenhi Grant-in-Aid for Early-Career Scientists JP23K13277, Grant-in-Aid for Scientific Research (B) JP22H01428 and JP21H01279, and the Urakami Foundation for Food and Food Culture Promotion.

References

[1] Crawley E F and De Luis J 1987 Use of piezoelectric actuators as elements of intelligent structures *AIAA Journal* **25** 1373–85

[2] Song G, Sethi V and Li H N 2006 Vibration control of civil structures using piezoceramic smart materials: A review *Eng Struct* **28** 1513–24

[3] Balamurugan V and Narayanan S 2001 Active vibration control of smart shells using distributed piezoelectric sensors and actuators *Smart Mater Struct* **10** 173–80

[4] Moheimani S O R, Halim D and Fleming A J 2003 *Spatial control of vibration - theory and experiments* (World Scientific Publishing Co. Pte. Ltd.)

[5] Li Y, Horowitz R and Evans R 2003 Vibration control of a PZT actuated suspension dual-stage servo system using a PZT sensor *IEEE Trans Magn* **39** 932–7

[6] Shan J, Liu H T and Sun D 2005 Slewing and vibration control of a single-link flexible manipulator by positive position feedback (PPF) *Mechatronics* **15** 487–503

[7] Kawai H 1969 The piezoelectricity of poly (vinylidene fluoride) *Jpn J Appl Phys* **8** 975–6

[8] Bailey T and Hubbard J E 1985 Distributed piezoelectric-polymer active vibration control of a cantilever beam *Journal of Guidance, Control, and Dynamics* **8** 605–11

[9] Wilkie W K, Bryant R G, High J W, Fox R L, Hellbaum R F, Jalink, Jr. A, Little B D and Mirick P H 2000 Low-cost piezocomposite actuator for structural control applications *Smart Structures and Materials 2000: Industrial and Commercial Applications of Smart Structures Technologies* vol 3991 (SPIE) pp 323–34

[10] Lu Q, Wang P and Liu C 2022 An analytical and experimental study on adaptive active vibration control of sandwich beam *Int J Mech Sci* **232** 107634

[11] Zhang Y, Zhang X and Xie S 2010 Adaptive vibration control of a cylindrical shell with laminated PVDF actuator *Acta Mech* **210** 85–98

[12] Sohn J W, Choi S B and Kim H S 2011 Vibration control of smart hull structure with optimally placed piezoelectric composite actuators *Int J Mech Sci* **53** 647–59

[13] Kwak M K, Heo S and Jeong M 2009 Dynamic modelling and active vibration controller design for a cylindrical shell equipped with piezoelectric sensors and actuators *J Sound Vib* **321** 510–24

[14] Rosset S, Araromi O A, Schlatter S and Shea H R 2016 Fabrication process of silicone-based dielectric elastomer actuators *Journal of Visualized Experiments*

[15] Romasanta L J, Lopez-Manchado M A and Verdejo R 2015 Increasing the performance of dielectric elastomer actuators: A review from the materials perspective *Prog Polym Sci* **51** 188–211

[16] He L, Lou J, Du J and Wang J 2017 Finite bending of a dielectric elastomer actuator and pre-stretch effects *Int J Mech Sci* **122** 120–8

[17] Wissler M and Mazza E 2005 Modeling and simulation of dielectric elastomer actuators *Smart Mater Struct* **14** 1396–402

[18] Hirai T, Sadatoh H, Ueda T, Kasazaki T, Kurita Y, Hirai M and Hayashi S 1996 Polyurethane-elastomer-actuator *Die Angewandte Makromolekulare Chemie* **240** 221–9

[19] Rosset S, O'Brien B M, Gisby T, Xu D, Shea H R and Anderson I A 2013 Self-sensing dielectric elastomer actuators in closed-loop operation *Smart Mater Struct* **22**

[20] Pelrine R, Kornbluh R, Pei Q and Joseph J 2000 High-speed electrically actuated elastomers with strain greater than 100% *Science* **287** 836–9

[21] Moretti G, Rizzello G, Fontana M and Seelecke S 2022 High-frequency voltage-driven vibrations in dielectric elastomer membranes *Mech Syst Signal Process* **168**

[22] Shintake J, Rosset S, Schubert B, Floreano D and Shea H 2016 Versatile soft grippers with intrinsic electroadhesion based on multifunctional polymer actuators *Advanced Materials* **28** 231–8

[23] Shintake J, Cacucciolo V, Floreano D and Shea H 2018 Soft robotic grippers *Advanced Materials* **30**

[24] Shintake J, Cacucciolo V, Shea H and Floreano D 2018 Soft biomimetic fish robot made of dielectric elastomer actuators *Soft Robot* **5** 466–74

[25] Araromi O A, Gavrilovich I, Shintake J, Rosset S, Richard M, Gass V and Shea H R 2015 Rollable multisegment dielectric elastomer minimum energy structures for a deployable microsatellite gripper *IEEE/ASME Transactions on Mechatronics* **20** 438–46

[26] Anderson I A, Hale T, Gisby T, Inamura T, McKay T, O'Brien B, Walbran S and Calius E P 2010 A thin membrane artificial muscle rotary motor *Appl Phys A Mater Sci Process* **98** 75–83

[27] Chen Y, Zhao H, Mao J, Chirarattananon P, Helbling E F, Hyun N seung P, Clarke D R and Wood R J 2019 Controlled flight of a microrobot powered by soft artificial muscles *Nature* **575** 324–9

[28] Maffli L, Rosset S, Ghilardi M, Carpi F and Shea H 2015 Ultrafast all-polymer electrically tunable silicone lenses *Adv Funct Mater* **25** 1656–65

[29] Jia K, Wang M, Lu T and Wang T 2019 Linear control of multi-electrode dielectric elastomer actuator with a finite element model *Int J Mech Sci* **159** 441–9

[30] Imboden M, de Coulon E, Poulin A, Dellenbach C, Rosset S, Shea H and Rohr S 2019 High-speed mechano-active multielectrode array for investigating rapid stretch effects on cardiac tissue *Nat Commun* **10**

[31] Hosoya N, Masuda H and Maeda S 2019 Balloon dielectric elastomer actuator speaker *Applied Acoustics* **148** 238–45

[32] Hosoya N, Baba S and Maeda S 2015 Hemispherical breathing mode speaker using a dielectric elastomer actuator *J Acoust Soc Am* **138** EL424–8

[33] Gratz-Kelly S, Rizzello G, Fontana M, Seelecke S and Moretti G 2022 A multi-mode, multi-frequency dielectric elastomer actuator *Adv Funct Mater* **32**

[34] Hiruta T, Sasaki K, Hosoya N, Maeda S and Kajiwara I 2021 Firmness evaluation of postharvest pear fruit during storage based on a vibration experiment technique using a dielectric elastomer actuator *Postharvest Biol Technol* **182**

[35] Hiruta T, Hosoya N, Maeda S and Kajiwara I 2021 Experimental evaluation of frequency response and firmness

of apples based on an excitation technique using a dielectric elastomer actuator *Sens Actuators A Phys* **330**

[36] Sarban R, Jones R W, Mace B R and Rustighi E 2011 A tubular dielectric elastomer actuator: Fabrication, characterization and active vibration isolation *Mech Syst Signal Process* **25** 2879–91

[37] Karsten R, Lotz P and Schlaak H F 2011 Active suspension with multilayer dielectric elastomer actuator *Electroactive Polymer Actuators and Devices (EAPAD) 2011* vol 7976 (SPIE) p 79762M

[38] Kajiwara I, Kitabatake S, Hosoya N and Maeda S 2019 Design of dielectric elastomer actuators for vibration control at high frequencies *Int J Mech Sci* **157–158** 849–57

[39] Liu C, Xue Q, Xie S, Zhang Y and Luo Y 2023 Analytical and experimental studies on active vibration control of flexible thin-walled structure using multi-layer planar dielectric elastomer actuator *Sens Actuators A Phys* **357**

[40] Liu C, Wu Q, Su Y, Li Y and Xie S 2021 Multi-Layers Planar Dielectric Elastomer Actuator Toward Reducing Control Voltage in In-Plane Actuation Applications *Int J Appl Mech* **13** 2150044

[41] Hiruta T, Hosoya N, Maeda S and Kajiwara I 2021 Experimental validation of vibration control in membrane structures using dielectric elastomer actuators in a vacuum environment *Int J Mech Sci* **191**

[42] Young L G, Ramanathan S, Hu J and Pai P F 2005 Numerical and experimental dynamic characteristics of thin-film membranes *Int J Solids Struct* **42** 3001–25

[43] Lu Y, Shao Q, Amabili M, Yue H and Guo H 2020 Nonlinear vibration control effects of membrane structures with in-plane PVDF actuators: A parametric study *Int J Non Linear Mech* **122** 103466

[44] Zhang Y, Hiruta T, Kajiwara I and Hosoya N 2017 Active vibration suppression of membrane structures and evaluation with a non-contact laser excitation vibration test *Journal of Vibration and Control* **23** 1681–92

[45] Kajiwara I and Hosoya N 2011 Vibration testing based on impulse response excited by laser ablation *J Sound Vib* **330** 5045–57

[46] Wakata S, Hosoya N, Hasegawa N and Nishikino M 2022 Defect detection of concrete in infrastructure based on Rayleigh wave propagation generated by laser-induced plasma shock waves *Int J Mech Sci* **218** 107039

[47] Huda F, Kajiwara I, Hosoya N and Kawamura S 2013 Bolt loosening analysis and diagnosis by non-contact laser excitation vibration tests *Mech Syst Signal Process* **40** 589–604

[48] Haus H, Matysek M, Mößinger H and Schlaak H F 2013 Modelling and characterization of dielectric elastomer stack actuators *Smart Mater Struct* **22**

[49] Wissler M and Mazza E 2007 Electromechanical coupling in dielectric elastomer actuators *Sens Actuators A Phys* **138** 384–93

[50] Kofod G and Sommer-Larsen P 2005 Silicone dielectric elastomer actuators: Finite-elasticity model of actuation *Sens Actuators A Phys* **122** 273–83

[51] Pelrine R E, Kornbluh R D and Joseph J P 1998 Electrostriction of polymer dielectrics with compliant electrodes as a means of actuation *Sens Actuators A Phys* **64** 77–85

[52] Gu G Y, Gupta U, Zhu J, Zhu L M and Zhu X 2017 Modeling of viscoelastic electromechanical behavior in a soft dielectric elastomer actuator *IEEE Transactions on Robotics* **33** 1263–71

[53] Meng L, Bao W, Li F and Li H 2021 Hysteresis compensation control of a dielectric elastomer vibration isolator *Journal of Low Frequency Noise Vibration and Active Control* **40** 497–508